electronics

MDPI

Article

A Fast Power Lines RCS Calculation Method Combining IEDG with CM-SMWA

Chunfeng Chen [1,2], Changyu Hu [3] and Jianjiang Zhou [1,*]

[1] Key Laboratory of Radar Imaging and Microwave Photonics, Ministry of Education, Nanjing University of Aeronautics and Astronautics, Nanjing 210016, China
[2] Leihua Electronic Technology Research Institute, Aviation Industry Corporation of China, Wuxi 214063, China
[3] School of Electronic Information Engineering, Wuxi University, Wuxi 214063, China
* Correspondence: zjjee@nuaa.edu.cn

Abstract: The existing methods for calculating electromagnetic scattering can be used to obtain the RCS of power lines. However, these methods do not take advantage of the periodicity of power lines. We propose a fast electromagnetic scattering calculation method combining the integral equation discontinuous Galerkin (IEDG) method and the characteristic modes-Sherman–Morrison–Woodbury algorithm (CM-SMWA) exploiting the power lines with stranded structure. We adopt the IEDG to discretize the electric field integral equation (EFIE) so that the EFIE can deal with non-conformal grids and significantly increase the flexibility of the CM-SMWA. Combing with the periodic property of power lines, the modeling and grid generation shall be carried out within one cycle (stranding) of the power line, and the grids of the rest cycle of the power line can be spliced by translating the grid of the divided sections. The advantage of the proposed method lies in that only the CM of one segment needs to be calculated, and the result can be applied to other segments to avoid repeated calculation of the CMs. The simulation results of the RCS of power lines show that the calculation time of our method is cut down by 50% as compared to the conventional CM-SMWA.

Keywords: power lines; radar cross-section; characteristic mode; integral equation discontinuous Galerkin; Sherman–Morrison–Woodbury algorithm

check for updates

Citation: Chen, C.; Hu, C.; Zhou, J. A Fast Power Lines RCS Calculation Method Combining IEDG with CM-SMWA. *Electronics* **2023**, *12*, 757. https://doi.org/10.3390/electronics12030757

Academic Editor: Spyridon Nikolaidis

Received: 1 January 2023
Revised: 26 January 2023
Accepted: 30 January 2023
Published: 2 February 2023

1. Introduction

The most dangerous obstacle for helicopter flight is power lines [1,2]. Millimeter wave radar is one of the most effective means to detect power lines [3–6], where the characteristic of power lines Bragg echo [7–11] is the key to the successful detection of the power lines. The application of the learning-based power lines detection algorithms, such as support vector machines (SVMs) or convolutional neural networks (CNNs), depend on a large number of training samples, while the cost of collecting the real millimeter echo of power line is high, which limits the performance of learning-based detection methods. With the development of electromagnetic simulation technology, the electromagnetic scattering characteristics obtained by simulation are very realistic, and the radar cross-section (RCS) of power lines can be calculated, which relieves the demand of the learning-based power lines detection methods for a lot of RCS training samples.

The high-frequency method [12] proposed for electrically large size can quickly calculate the electromagnetic scattering of power lines. However, its accuracy is not easy to control. Compared with the high-frequency methods, the moment of method (MoM) [13] is able to obtain the RCS of power lines robustly. However, the computational complexity of the conventional MoM is too large, so it is suitable for the calculation of power lines with small electrical sizes. In the face of the demand for a lot of RCS training samples, it is necessary to develop accurate and efficient methods for obtaining the RCS of power lines.

In recent decades, many fast iterative algorithms for calculating RCS have been developed, such as the fast multipole method (FMM) [14,15], fast Fourier transform (FFT) [16,17],

and adaptive cross approximation (ACA) [18]. However, these algorithms recalculate the RCS of power lines for each incidence angle, which means that the above algorithms take a long time to calculate the RCS of power lines with multiple angles. In addition, they only accelerate matrix-vector products (MVPs), and keep the number of unknowns unchanged. Fast algorithms combing the characteristic modes (CMs) and the Sherman–Morrison–Woodbury formula-based algorithm (SMWA) have been proposed in [19], which is named CM-SMWA. The CMs are used as macro basis functions (MBF), which reduces the number of unknowns effectively, and the SMWA is employed to solve the reduced matrix directly and realizes the efficient solution of monostatic RCS of power lines with multiple plane waves. However, the CM-SMWA [19] does not use the periodic property of the stranded wire structure.

This paper proposes a fast RCS calculation method by exploiting the periodic stranded structure of power lines. First, we use the integral equation discontinuous Galerkin (IEDG) [20,21] to discretize the electric field integral equation (EFIE), so that the EFIE can deal with non-conformal grids and increase the flexibility of the CM-SMWA [19]. After the IEDG is added, the modeling and grid generation shall be carried out within one (stranding) repetition interval of the power line. The grids of the remaining parts of the power line can be spliced after the grid translation of the divided sections. It means that we only need to calculate the characteristic modes of one segment, which can be applied to other segments to avoid repeated calculations of the characteristic modes of different segments. Furthermore, the translation invariance of impedance elements can be used to optimize the generation of reduced matrix and enhance the generation efficiency of the reduced matrix. In order to simplify the expression, the RCS calculation method proposed in this paper is named IEDG-CM-SMWA. The contributions of this paper are as follows:

(1) It is the first time IEDG with CM-SMWA are combined, and the corresponding combining method is given;

(2) The periodicity of power lines is introduced to enhance the calculation efficiency of the electromagnetic scattering of power lines;

(3) The feasibility and effectiveness of our proposed IEDG-CM-SMWA are verified sufficiently by simulated power lines data.

In this paper, the simulation results of the IEDG-CM-SMWA are compared with the simulation results of the MoM and the CM-SMWA to clarify the specific embodiment of the merits of the proposed method.

The rest of this paper is organized as follows: Section 2 briefly introduces the power line RCS calculation method based on the CM-SMWA. Section 3 presents the proposed fast RCS calculation method combining IEDG and CM-SMWA in detail. In Section 4, simulated power line data are used to verify the performance of the IEDG-CM-SMWA. Section 5 summarizes the conclusions of this paper.

2. CM-SMWA

The metal power lines can be regarded as perfect electrical conductors (PEC), as shown in Figure 1. According to the equivalence principle and the boundary conditions of the PEC surface, we can obtain the EFIE for solving the electromagnetic scattering from power lines, as follows [13]:

$$\hat{\mathbf{n}} \times \hat{\mathbf{n}} \times \left(-j\omega\mu_0 \int_s G(\mathbf{r},\mathbf{r}')\mathbf{J}(\mathbf{r}')ds' - \nabla \frac{1}{j\omega\varepsilon_0} \int_s G(\mathbf{r},\mathbf{r}')\nabla' \cdot \mathbf{J}(\mathbf{r}')ds' \right) = \hat{\mathbf{n}} \times \hat{\mathbf{n}} \times \mathbf{E}^i(\mathbf{r})\varepsilon_0 \quad (1)$$

where $\mathbf{J}(\mathbf{r}')$ denotes the unknown surface current, $\hat{\mathbf{n}}$ is the unit normal direction of the PEC surface. The Green's function in free space is $G(\mathbf{r},\mathbf{r}')$, $\mathbf{r}$ and $\mathbf{r}'$ are the position vectors of field point and source point, ε_0 denotes the permittivity, represents permeability in free space, and represents an imaginary unit.

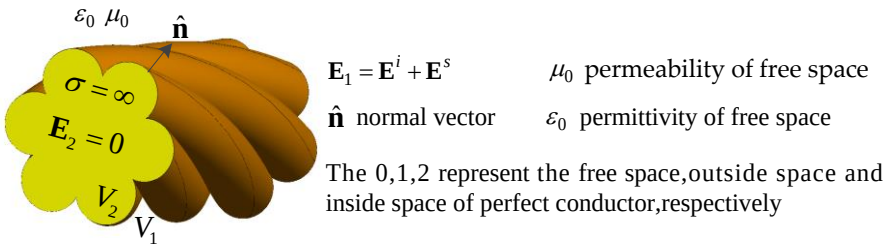

Figure 1. Diagrammatic sketch of a PEC power line.

The impedance matrix equation of MoM can be obtained by using the RWG basis function [22] to expand $\mathbf{J}(\mathbf{r}')$ in Formula (1) and using the Galerkin method:

$$\mathbf{ZI} = \mathbf{V} \tag{2}$$

The element in $\mathbf{Z}$ and $\mathbf{V}$ is shown in Equations (3) and (4), respectively [13]:

$$Z_{mn}^{EFIE} = jk\eta \int_{T_m} \int_{T_n} G(\mathbf{r}, \mathbf{r}') \left(\mathbf{f}_m(\mathbf{r}) \cdot \mathbf{f}_n(\mathbf{r}') - \frac{1}{k^2} \nabla \cdot \mathbf{f}_m(\mathbf{r}) \nabla' \cdot \mathbf{f}_n(\mathbf{r}') \right) ds' ds \tag{3}$$

$$V_m = \int_{T_m} \mathbf{f}_m(\mathbf{r}) \cdot \mathbf{E}^i(\mathbf{r}) ds \tag{4}$$

In (3), $\eta = \sqrt{\mu_0/\varepsilon_0}$ and k represent the wave impedance and the wave number, respectively. $\mathbf{f}_m(\mathbf{r})$ and $\mathbf{f}_n(\mathbf{r})$ denote the m-th and n-th RWG basis functions [22]. T_m and T_n represent the domain of $\mathbf{f}_m(\mathbf{r})$ and $\mathbf{f}_n(\mathbf{r})$, respectively. After Z_{mn} and V_m are obtained, the current I_n in (2) can be obtained, and finally $\mathbf{J}(\mathbf{r})$ can be calculated.

However, for electrically large power lines, the direct solution of (2) is very time- and memory-consuming. To solve this problem, a fast direct algorithm, CM-SMWA is proposed in [19]. The method first groups the basis functions of power lines along the long axis and assumes that the number of groups is B, then the MoM matrix equation is readjusted to the following forms:

$$\begin{bmatrix} \mathbf{Z}_{11} & \mathbf{Z}_{12} & \cdots & \mathbf{Z}_{1B} \\ \mathbf{Z}_{21} & \mathbf{Z}_{22} & \cdots & \mathbf{Z}_{2B} \\ \vdots & \vdots & \ddots & \vdots \\ \mathbf{Z}_{B1} & \mathbf{Z}_{B2} & \cdots & \mathbf{Z}_{BB} \end{bmatrix} \begin{bmatrix} \mathbf{I}_1 \\ \mathbf{I}_2 \\ \vdots \\ \mathbf{I}_B \end{bmatrix} = \begin{bmatrix} \mathbf{V}_1 \\ \mathbf{V}_2 \\ \vdots \\ \mathbf{V}_B \end{bmatrix} \tag{5}$$

According to [23,24], using the self-impedance matrix of each block, the characteristic modes of each block can be obtained by solving the generalized eigenvalue equation:

$$\mathbf{X}_{ii} \cdot \mathbf{J}_i^{CM}(:, n) = \lambda_n \mathbf{R}_{ii} \cdot \mathbf{J}_i^{CM}(:, n) \tag{6}$$

where, $\mathbf{X}_{ii} = imag(\mathbf{Z}_{ii})$, $\mathbf{R}_{ii} = real(\mathbf{Z}_{ii})$, $\mathbf{J}_i^{CM}(:, n)$ represent the nth characteristic mode on the i-th block, and λ_n represents the eigenvalue corresponding to the n-th characteristic mode.

Then, (5) can be compressed by using the characteristic modes into $\mathbf{Z}^{CM}\boldsymbol{\alpha} = \mathbf{V}^{CM}$,

$$\begin{bmatrix} \mathbf{Z}_{11}^{CM} & \mathbf{Z}_{12}^{CM} & \cdots & \mathbf{Z}_{1B}^{CM} \\ \mathbf{Z}_{21}^{CM} & \mathbf{Z}_{22}^{CM} & \cdots & \mathbf{Z}_{2B}^{CM} \\ \vdots & \vdots & \ddots & \vdots \\ \mathbf{Z}_{B1}^{CM} & \mathbf{Z}_{B2}^{CM} & \cdots & \mathbf{Z}_{BB}^{CM} \end{bmatrix} \begin{bmatrix} \boldsymbol{\alpha}_1 \\ \boldsymbol{\alpha}_2 \\ \vdots \\ \boldsymbol{\alpha}_B \end{bmatrix} = \begin{bmatrix} \mathbf{V}_1^{CM} \\ \mathbf{V}_2^{CM} \\ \vdots \\ \mathbf{V}_B^{CM} \end{bmatrix} \tag{7}$$

where

$$\mathbf{Z}_{ij}^{CM} = (\mathbf{J}_i^{CM})^T \mathbf{Z}_{ij} \mathbf{J}_j^{CM} \tag{8}$$

$$\mathbf{V}_i^{CM} = (\mathbf{J}_i^{CM})^T \mathbf{V}_i \tag{9}$$

$(\mathbf{J}_i^{CM})^T$ indicates the transposition of $\mathbf{J}_i^{CM}$.

The SMWA fast direct algorithm [25–28] is used to solve (7), and $\boldsymbol{\alpha} = [\alpha_1^T, \alpha_2^T, \ldots, \alpha_B^T]^T$ is calculated. The current finally obtained is $\mathbf{I} = \mathbf{J}^{CM}\boldsymbol{\alpha}$, where $\mathbf{J}^{CM}$ is

$$\mathbf{J}^{CM} = \begin{bmatrix} \mathbf{J}_1^{CM} & & & \\ & \mathbf{J}_2^{CM} & & \\ & & \ddots & \\ & & & \mathbf{J}_B^{CM} \end{bmatrix} \tag{10}$$

As can be seen from (6), the characteristic modes $\mathbf{J}_1^{CM}$~$\mathbf{J}_B^{CM}$ are calculated separately, and the calculation takes a long time. Note that the structural feature of the power line is periodic symmetry, so we can divide the power line into B segments at equal intervals according to the period. It is desired that we only need to calculate the characteristic modes of one section of power line, while the characteristic modes of other sections can be obtained by periodicity. If we want to take advantage of the periodic characteristics of power lines, we must make the grid of power line lines in each cycle exactly the same. Then, in the expanded mesh, the mesh of two adjacent periods in contact is likely to have mismatched nodes. In other words, the expanded mesh is non-conformal. Because the traditional MoM and CM-SMWA can not deal with non-conformal mesh, they can not take advantage of the periodicity of power lines. The proposed IEDG-CM-SMWA can calculate power lines with non-conformal mesh by introducing IEDG.

3. RCS Calculation Method of Power Line Combining IEDG and CM-SMWA

3.1. IEDG

In order to solve the above problem (non-conformal mesh problem), we utilize the IEDG [20,21] to solve the integral equation, and realize the power line calculation in the case of mismatched nodes of the triangular grid. Assume that the symmetric period is P, as shown in Figure 2:

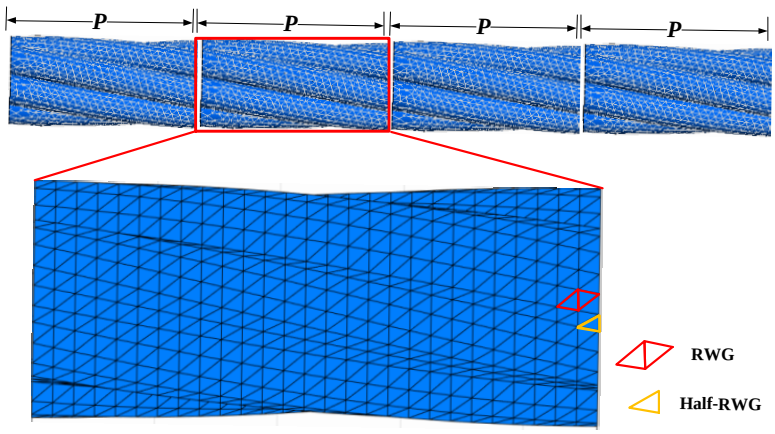

Figure 2. RWG and half-RWG after periodic segmentation of power line.

As shown in Figure 1, each period contains RWGs [22] inside and half-RWGs at the boundary. Half-RWG [29] adopted by the IEDG is presented in Figure 3:

Half-RWG has only one triangle, and the n-th half-RWG is expressed as:

$$\mathbf{f}_n(\mathbf{r}) = \begin{cases} \frac{l_n}{2A_n}\boldsymbol{\rho}_n(\mathbf{r}) & \mathbf{r} \in T_n \\ 0 & else \end{cases} \tag{11}$$

where, T_n refers to the triangle of the n-th half RWG basis function, A_n refers to the area of the triangle, $\boldsymbol{\rho}_n(\mathbf{r})$ refers to the vector that the triangle node points to the point inside

the triangle, l_n refers to the side length, and $\hat{\mathbf{n}}_n(\mathbf{r})$ refers to the normal vector pointing out of T_n.

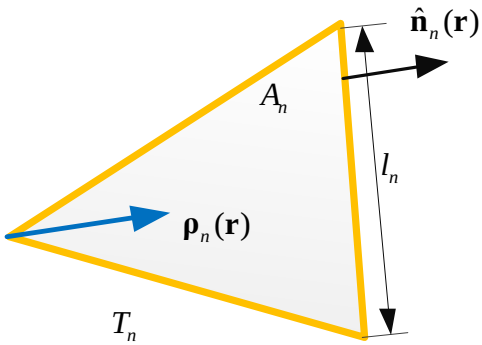

Figure 3. Schematic diagram of half-RWG basis function.

The surface charge density can be obtained by calculate the divergence of (11).

$$\nabla \cdot \mathbf{f}_n(\mathbf{r}) = \begin{cases} \frac{l_n}{A_n} & \mathbf{r} \in T_n \\ 0 & else \end{cases} \tag{12}$$

Two adjacent half RWG basis functions with a part of the common side length do not meet the requirements of current continuity. The influence of the penalty terms is to avoid the current discontinuity caused by non-conformal mesh. In the case of lacking the penalty terms, the current between non-conformal mesh can not be guaranteed to be continuous, which will lead to large calculation error of RCS. In the case of introducing the penalty terms, the penalty terms can ensure the continuity of current between non-conformal mesh, to avoid the RCS calculation error caused by discontinuous current. Therefore, it is necessary to add charge penalty term and potential penalty term according to the literature [20]. Then the corresponding impedance element becomes

$$\mathbf{Z}_{mn} = jk\eta \int_{T_m} \int_{T_n} \mathbf{f}_m(\mathbf{r}) \cdot \left(\mathbf{I} + \frac{\nabla\nabla}{k^2} \right) G(\mathbf{r}, \mathbf{r}') \cdot \mathbf{f}_n(\mathbf{r}') ds' ds + \mathbf{R}^p_{mn} + \mathbf{R}^c_{mn} \tag{13}$$

where, $\mathbf{R}^p_{mn}$ is the potential penalty term and $\mathbf{R}^c_{mn}$ is the charge penalty term [20].

$$\mathbf{R}^p_{mn} = \frac{j\eta}{k} \int_{C_m} \left(\hat{\mathbf{n}}_m \cdot \mathbf{f}_m(\mathbf{r}) \right) \int_{C_n} \left(\hat{\mathbf{n}}_n \cdot \mathbf{f}_n(\mathbf{r}') G(\mathbf{r}, \mathbf{r}') \right) dl_n dl_m \tag{14}$$

$$\mathbf{R}^c_{mn} = \frac{j\eta\beta}{k} \int_{C_m} \left(\hat{\mathbf{n}}_m \cdot \mathbf{f}_m(\mathbf{r}) \right) \left(\hat{\mathbf{n}}_n \cdot \mathbf{f}_n(\mathbf{r}') \right) dl_m \tag{15}$$

C_m and C_n are the contour boundaries of T_m and T_n. β is the coefficient of charge compensation term, and its value is as follows:

$$\beta = \frac{\alpha}{h} \tag{16}$$

h is the average length of the mesh [20]. In this paper, the value of α is taken as 0.1.

By further derivation of (13), it can be obtained that the expression of the EFIE impedance element in the IEDG [20] is:

$$\begin{aligned}\mathbf{Z}_{mn} &= jk\eta \int_{T_m}\int_{T_n} G(\mathbf{r},\mathbf{r}')\Big(\mathbf{f}_m(\mathbf{r})\cdot\mathbf{f}_n(\mathbf{r}') - \tfrac{1}{k^2}\nabla\cdot\mathbf{f}_m(\mathbf{r})\nabla'\cdot\mathbf{f}_n(\mathbf{r}')\Big)ds'ds \\ &+\tfrac{j\eta}{k}\int_{T_m}\nabla\cdot\mathbf{f}_m(\mathbf{r})\int_{C_n} G(\mathbf{r},\mathbf{r}')\hat{\mathbf{n}}_n\cdot\mathbf{f}_n(\mathbf{r}')dl'ds \\ &+\tfrac{j\eta}{k}\int_{C_m}\hat{\mathbf{n}}_m\cdot\mathbf{f}_m(\mathbf{r})\int_{T_n} G(\mathbf{r},\mathbf{r}')\nabla'\cdot\mathbf{f}_n(\mathbf{r}')ds'dl \\ &+\tfrac{j\eta\beta}{k}\int_{C_m}\Big(\hat{\mathbf{n}}_m\cdot\mathbf{f}_m(\mathbf{r})\Big)\Big(\hat{\mathbf{n}}_n\cdot\mathbf{f}_n(\mathbf{r}')\Big)dl_m\end{aligned} \tag{17}$$

When the RWG basis function and the half-RWG basis function are mixed in the MoM, the expressions of impedance matrix elements will be divided into four cases [20,21]:

As shown in Table 1, under different combinations of full RWG and half RWG, the summation term in (17) is used to calculate the impedance matrix as follows:

Table 1. Impedance Calculation under Different Combinations of RWG and Half-RWG.

Cases	*m*	*n*	Summation Terms
1	RWG	RWG	1
2	RWG	half-RWG	1, 2
3	half-RWG	RWG	1, 3
4	half-RWG	half-RWG	1, 2, 3, 4

(1) When the m-th and n-th basis function are the full RWG functions, the impedance matrix is obtained by calculating the first term in Equation (17);

(2) When the m-th and n-th basis functions are the full RWG and half-RWG, respectively, the impedance matrix is obtained by calculating the first and second terms in Equation (17);

(3) When the m-th and n-th basis functions are the half-RWG and full RWG, respectively, the impedance matrix is obtained by calculating the first and third terms in Equation (17);

(4) When the m-th and n-th basis functions are the half-RWG functions, calculate all items in (17) to obtain the impedance matrix.

3.2. Power Line RCS Calculation by IEDG with CM-SMWA

According to (17), the grouped near-field matrix $\mathbf{Z}_{11}$ can be calculated. Since the expression of the basis function in each segment of near-field matrix $\mathbf{Z}_{ii}$ is the same, it is easy to obtain all near-field matrices $\mathbf{Z}_{ii} = \mathbf{Z}_{11}$, and similarly, the far-field matrix $\mathbf{Z}_{12} = \mathbf{Z}_{23} = \ldots \mathbf{Z}_{B-1,B}$ can be calculated. As shown in Figure 4, it is only necessary to calculate $\mathbf{Z}_{11}, \mathbf{Z}_{12}, \mathbf{Z}_{13} \ldots \mathbf{Z}_{1B}$, and further transpose each element of the upper triangle of the far-field matrix to obtain the value of each element of the lower triangle of the impedance matrix, and then obtain $\mathbf{Z}$.

The CM is applicable to the itself mode of any electromagnetic structure, and only related to the shape and material of the structure itself. When calculating the characteristic modes, because of $\mathbf{Z}_{ii} = \mathbf{Z}_{11}$, so $\mathbf{J}_1 = \mathbf{J}_2 = \ldots \mathbf{J}_B$. Therefore, our method only needs to calculate the characteristic modes of $\mathbf{Z}_{11}$ to obtain the characteristic modes of all groups. Compared with the conventional CM-SMWA, the calculation time of characteristic modes is reduced by B times by the proposed method.

After obtaining $\mathbf{Z}^{CM}$, the CM method is used to improve efficiency of the SMWA [25–28]. The current and RCS are finally obtained.

As shown in Figure 5, the steps of the IEDG-CM-SMWA are as follows:

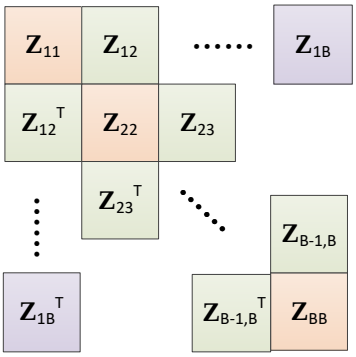

Figure 4. Impedance matrix diagram. The impedance submatrices with the same color have the same impedance elements, and they need to be calculated only once.

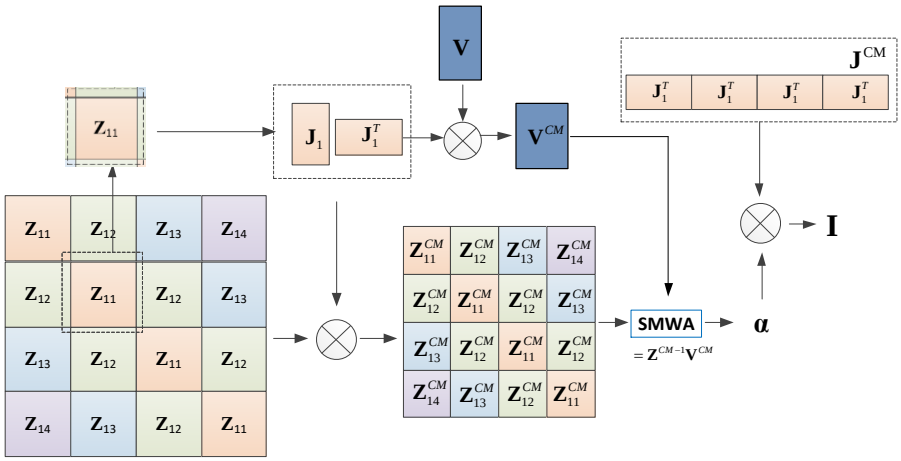

Figure 5. Schematic Diagram of IEDG-CM-SMWA Algorithm Steps.

Step 1: divide the power line into B sections at equal intervals P along the long axis. Calculate the impedance submatrices $\mathbf{Z}_{11}, \mathbf{Z}_{12}, \ldots \mathbf{Z}_{1B}$ in the first row, and calculate the characteristic modes of the expanded $\mathbf{Z}_{11}$ to obtain $\mathbf{J}_1$;

Step 2: bring $\mathbf{J}_1$ into matrix $\mathbf{Z}_{11}, \mathbf{Z}_{12}, \ldots \mathbf{Z}_{1B}$, calculate $\mathbf{Z}_{11}^{CM}, \mathbf{Z}_{12}^{CM}, \ldots \mathbf{Z}_{1B}^{CM}$, and calculate $\mathbf{V}_i^{CM} = (\mathbf{J}_1)^T \mathbf{V}_i$. In order to reduce memory consumption, every time a submatrix $\mathbf{Z}_{1i}$ in $\mathbf{Z}_{11}, \mathbf{Z}_{12}, \ldots \mathbf{Z}_{1B}$ is calculated, a $\mathbf{Z}_{1i}^{CM}$ is calculated. After that, $\mathbf{Z}_{11}$ is cleared, and then $\mathbf{Z}_{12}$ is calculated. Clear $\mathbf{Z}_{12} \ldots$ until all $\mathbf{Z}_{11}^{CM}, \mathbf{Z}_{12}^{CM}, \ldots \mathbf{Z}_{1B}^{CM}$ are calculated;

Step 3: Use $\mathbf{Z}_{11}^{CM}, \mathbf{Z}_{12}^{CM}, \ldots \mathbf{Z}_{1B}^{CM}$ to form matrix $\mathbf{Z}^{CM}$, and compute $\mathbf{Z}^{CM-1}$ by using the SMW formula [19];

Step 4: Calculate $\boldsymbol{\alpha}$ using the SMWA and then calculate the current $\mathbf{I} = \mathbf{J}^{CM}\boldsymbol{\alpha}$. Calculate the RCS of power lines according to the current.

4. Experimental Results and Analysis

4.1. Simulated Models

In our work, we used the simulated power lines to verify the performance of the IEDG-CM-SMWA for power line RCS calculation. The model of the simulated power line is LGJ50-8, and the LGJ50-8 has a steel core and six external aluminum strands. The physical structure of the power line is shown in Figure 6:

In Figure 6, ρ is the distance between two strands, P is the winding cycle of a single strand, D is the diameter of the power line, and d is the diameter of the single aluminum stranded wire. These parameters of the power line LGJ50-8 are given in Table 2.

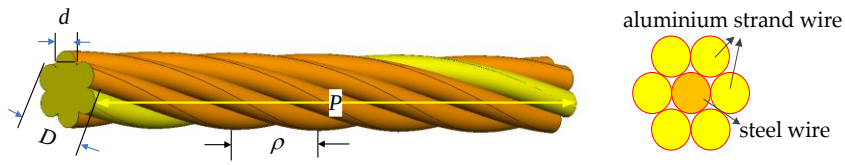

(**a**) (**b**)

Figure 6. Simulated power line LGJ50-8. (**a**) The surface. (**b**) The cross-section.

Table 2. Parameters setting of power line LGJ50-8.

Model	Steel Core	Outer Aluminum Strand/*d*	Diameter *D*	*P*	*ρ*
LGJ50-8	1	6/3.2 mm	9.55 mm	138 mm	23 mm

4.2. Evaluation Indicators

In this paper, we use the computational time and accuracy to measure the performance of the new method. In particular, we use RCS relative error to measure the accuracy of the new method in calculating RCS. The formula of relative error is as follows:

$$\frac{\sqrt{\sum_{n=1}^{N_\theta} \left|\sigma(n) - \sigma_s^0(n)\right|^2}}{\sqrt{\sum_{n=1}^{N_\theta} \left|\sigma_s^0(n)\right|^2}} \tag{18}$$

where N_θ denotes the number of angles, and σ_s^0 is the reference value of RCS.

4.3. Numerical Calculation Comparison

In this paper, 35 GHz and 76 GHz frequencies under horizontal–horizontal (H–H) and vertical–vertical (V–V) polarities are selected for simulation to verify the advantages of the proposed algorithm. The 35 GHz frequency is low, which is a common anti-collision frequency band for large and medium-sized helicopters. And 35 GHz has a stronger all-weather capability due to its lower frequency. The 76 GHz millimeter wave radar can be used as low-cost or on-chip radar [30,31]. Many basis functions need to be calculated because the wavelength of this frequency is very short.

(1) Simulation of incident wave frequency at 35 GHz

The length of power line 1 shown in Table 2 is 184 mm, with eight recurrences in total. The polarization mode of the incident wave is V–V polarization, and the frequency is set to 35 GHz. The ACA tolerance used in the SMWA is set to 1×10^{-4}. For the IEDG-CM-SMWA method in this paper, each interval can be divided into 2880 full RWGs and 152 half-RWGs. The CM-SMWA uses 23292 full RWGs. The power line is divided into eight segments using a three-level binary tree. The number of characteristic modes in each group is arranged as 700.

Use IEDG-CM-SMWA, CM-SMWA, and MoM to calculate the RCS of the power line, and the calculation results are shown in Figure 7.

We can find from Figure 7 that the RCS of the Bragg echo points of different algorithms under the V–V polarization condition is relatively consistent, and there is only a large relative error of about −40 dBsm. For the same absolute error, the relative error is relatively large, where the actual RCS value is small. However, when the power line RCS is about −40 dB, the RCS is generally smaller than the radar receiving noise in practice, which is easy to submerge by noise, and does not affect the effectiveness of RCS calculation.

The quantitative evaluation indexes in Section 4.2 are used to analyze the RCS of power lines obtained by the three algorithms, as shown in Table 3:

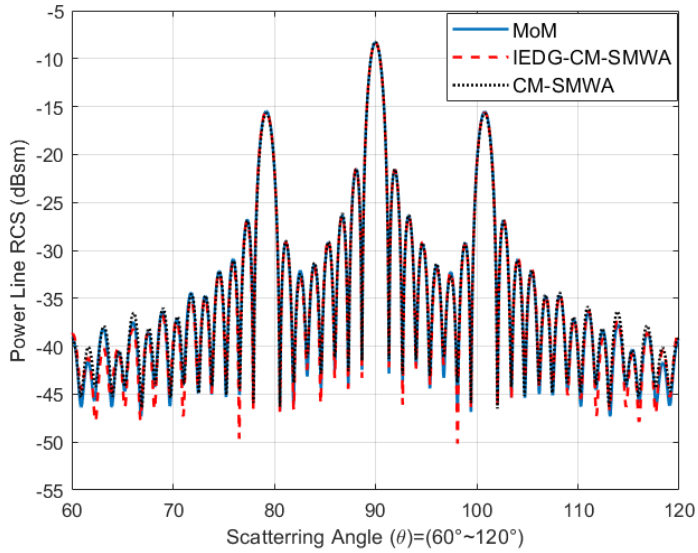

Figure 7. RCS of the power line calculated by IEDG−CM−SMWA, CM−SMWA, and MoM under the same impedance matrix grouping. The abscissa represents the incident angle of electromagnetic wave, and the ordinate represents the RCS of power line. The black dotted line is the result of CM-SMWA, the blue solid line is the result of MoM, and the calculation result of IEDG-CM-SMWA is the orange dotted line.

Table 3. Comparations of the three methods for calculating the power line LGJ50-8.

Methods	Total Time	Relative Error
MoM	7.3 min	–
CM-SMWA	6.3 min	1.2%
IEDG-CM-SMWA	**1.9 min**	1.2%

It can be seen from Table 3 that the IEDG-CM-SMWA has greater advantages in terms of calculation speed under the same grouping conditions. We can find from the relative error column in Table 3 that the IEDG-CM-SMWA is basically consistent with the results of the conventional MoM and CM-SMWA.

Further verification under different groups was carried out. The CM-SMWA is with 32 groups, and the characteristic modes in each group is 400. The IEDG-CM-SMWA method was still divided into eight groups. Use the IEDG-CM-SMWA, CM-SMWA, and MoM to calculate the RCS of the power line, and calculation results are given in Figure 8.

We can see from Figure 8 that under the V–V polarization condition, when the grouping is different, the RCS of the Bragg echo points of different algorithms is relatively consistent.

The quantitative evaluation indexes in Section 4.2 are used to analyze the RCS of power lines obtained by the three algorithms, as shown in Table 4:

Comparing the computational time of the CM-SMWA in Table 3 and that of the CM-SMWA in Table 4, we can find that the CM-SMWA divides the matrix into smaller parts, which will reduce the calculation time for this example. However, the IEDG-CM-SMWA proposed in this paper still saves time compared with the traditional CM-SMWA.

To illustrate the difference between the RCS of the power line and the PEC cylinder, we calculate the RCS of a cylinder with the same length and diameter as the power line LGJ50-8, as shown in Figure 9.

We can see from Figure 9 that the RCS of the cylinder is close to the RCS of the power line at the normal incidence (incidence angle 90°). However, the RCS of the power line has Bragg points at about 10.7° away from the normal incidence. The position of the Bragg point is determined by the stranding period of the power line. When the wave path difference of the incident waves, that reaches the adjacent strands, is an integral multiple of

0.5 λ, the scattering echoes will be enhanced [19], but the smooth cylinder does not have Bragg points.

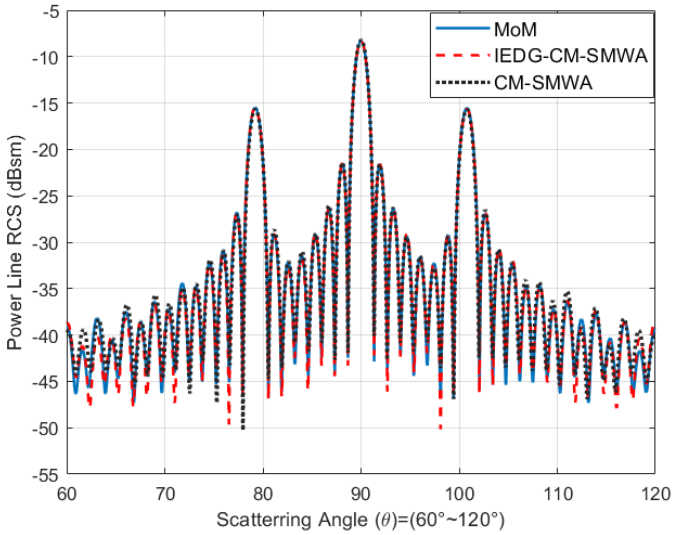

Figure 8. RCS of the power line calculated by IEDG−CM−SMWA, CM−SMWA, and MoM under different impedance matrix grouping.

Table 4. RCS simulation performance of power line LGJ50-8 with divides the matrix into smaller parts obtained by three methods.

Methods	Total Time	Relative Error
MoM	7.3 min	–
CM-SMWA	4.2 min	4.3%
IEDG-CM-SMWA	**1.9 min**	**1.2%**

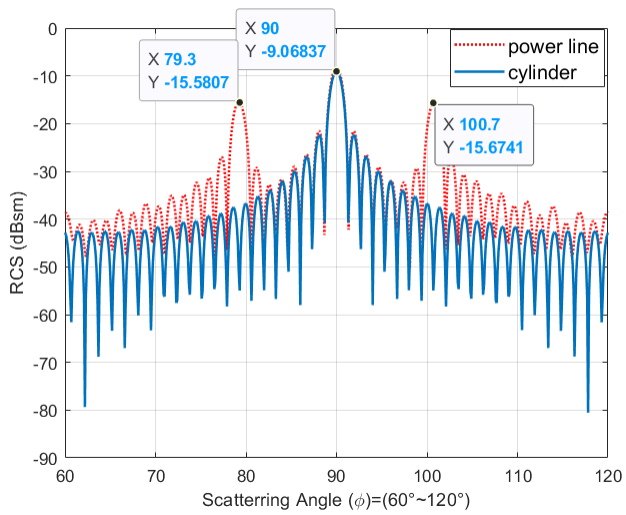

Figure 9. RCS comparison between power line and cylinder with the same length and diameter at 35 GHz.

(2) Simulation of incident wave frequency at 76 GHz

For the same power line as in Example 1, under the condition of 76 GHz frequency, the target is discretized by RWG with an average size of 0.1 wavelength. Because of the high frequency, the grid is smaller, and 110,370 RWGs are used. The level of the binary tree of the CM-SMWA method is 7, and the power line is divided into 128 segments. The IEDG-CM-SMWA is also eight segments. The simulation results are given in Figure 10.

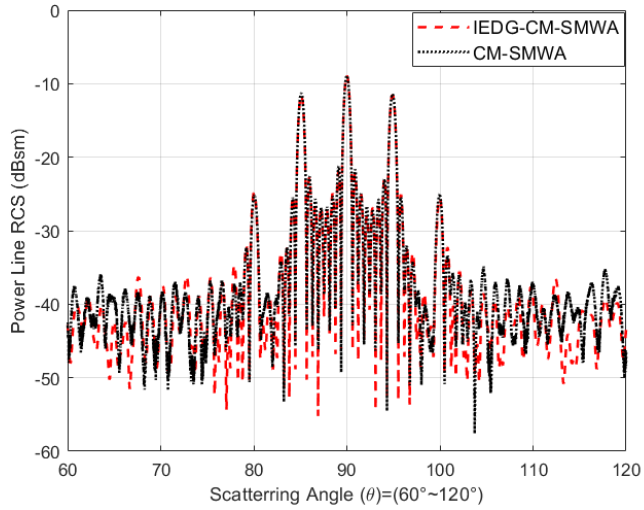

Figure 10. RCS of the power line computed by IEDG−CM−SMWA and CM-SMWA under the condition of H–H polarization at 76 GHz.

We can see from Figure 10 that the RCS of the Bragg echo points of the IEDG-CM-SMWA and the CM-SMWA are relatively consistent under the H–H polarization condition.

We can find from Table 5 that the RCS relative error of the two methods is 2.8%, which is very close. The calculation time of the method proposed in this paper is still faster.

Table 5. RCS simulation performance of power line LGJ50-8 under the 76 GHz(H−H).

Methods	Total Time	Relative Error
CM-SMWA	56.3 min	
IEDG-CM-SMWA	**28.1 min**	**2.8%**

In order to further demonstrate the properties of power line with different polarizations, the V–V polarization RCS simulation is also carried out. The RCS results are shown in Figure 11.

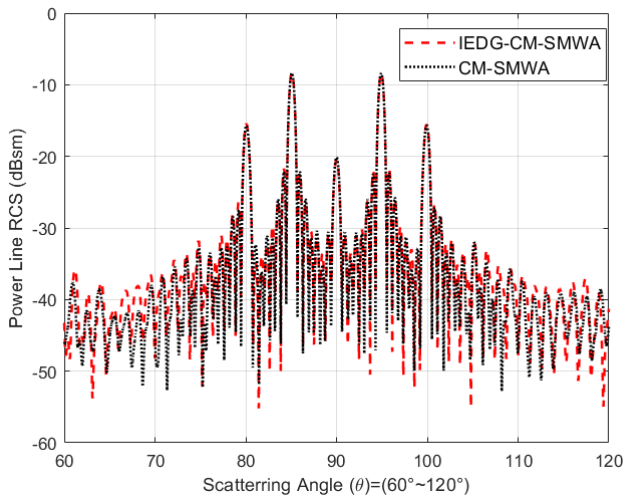

Figure 11. RCS of the power line computed by the IEDG-CM-SMWA and CM-SMWA under the V–V polarization of 76 GHz.

We can see from Figure 11 that under the V–V polarization condition, the RCS of the Bragg echo points of the IEDG-CM-SMWA and the CM-SMWA are also relatively consistent.

It can be seen from Table 6 that the IEDG-CM-SMWA can still maintain the leading speed under different polarization conditions. It shows that the proposed method has strong applicability, and is able to satisfy the requirements of power line detection, and has greater advantages in computational efficiency compared with the previous method.

Table 6. RCS simulation performance of power line LGJ50-8 under the 76 GHz(V–V).

Methods	Total Time	Relative Error
CM-SMWA	57.9 min	
IEDG-CM-SMWA	**26.4 min**	**3.1%**

5. Conclusions

This paper proposes a fast power line RCS calculation method combining IEDG and CM-SMWA. The calculation results of power line RCS show that the new method is feasible and effective. The IEDG combined with the periodicity of power lines can significantly reduce the time consumption of RCS calculation. Compared with the conventional CM-SMWA, the presented method has the advantages in RCS calculation time. The proposed method has the potential to complete RCS simulation more quickly under limited resources, and be better applied to generate large-scale power line RCS samples.

Author Contributions: Conceptualization, C.C. and J.Z.; methodology, C.C.; software, C.C.; validation, C.C.; investigation, J.Z.; writing—original draft preparation, C.C.; writing—review and editing, J.Z. and C.H. All authors have read and agreed to the published version of the manuscript.

Funding: This work was supported in part by the National Natural Science Foundation of China under Grant 61801212, "Light of Taihu Lake" scientific and technological breakthrough (basic research) K20221049, and in part by Key Laboratory of Radar Imaging and Microwave Photonics (Nanjing Univ. Aeronaut. Astronaut.), Ministry of Education, Nanjing, China.

Institutional Review Board Statement: Not applicable.

Informed Consent Statement: Not applicable.

Data Availability Statement: The study did not report any data.

Conflicts of Interest: The authors declare no conflict of interest.

References

1. Chandrasekaran, R.; Payan, A.P.; Collins, K.B. Helicopter Wire Strike Protection and Prevention Devices: Review, Challenges, And Recommendations. *Aerosp. Sci. Technol.* **2020**, *98*, 105665. [CrossRef]
2. Rao, A.H.; Marais, K. High Risk Occurrence Chains in Helicopter Accidents. *Reliab. Eng. Syst. Saf.* **2018**, *170*, 83–98. [CrossRef]
3. Goshi, D.S.; Case, T.J.; Mckitterick, J.B.; Long, Q.B. Multifunctional Millimeter Wave Radar System for Helicopter Safety. *Proc. SPIE—Int. Soc. Opt. Eng.* **2012**, *8361*, 173.
4. Kumar, B.A.; Ghose, D. Radar-Assisted Collision Avoidance/Guidance Strategy for Planar Flight. *IEEE Trans. Aerosp. Electron. Syst.* **2001**, *37*, 77–90. [CrossRef]
5. Goshi, D.S.; Mai, K.; Liu, Y.; Bui, L. A Millimeter-Wave Sensor Development System for Small Airborne Platforms. In Proceedings of the IEEE National Radar Conference Proceedings, Atlanta, GA, USA, 7–11 May 2012; pp. 510–515.
6. Migliaccio, C.; Nguyen, B.D.; Pichot, C.; Yonemoto, N.; Yamamoto, K.; Yamada, K.; Nasui, H.; Mayer, W.; Gronau, A.; Menzel, W. Millimeter-Wave Radar for Rescue Helicopters. In Proceedings of the International Conference on Control, Kaunas, Lithuania, 4–5 May 2006; pp. 1–6.
7. Al-Khatib, H.H. Laser and Millimeter-Wave Backscatter of Transmission Cables. In Proceedings of the Technical Symposium, Washington, DC, USA, 13–15 October 1982.
8. Sarabandi, K.; Park, M. Millimeter-Wave Radar Phenomenology of Power Lines and a Polarimetric Detection Algorithm. *IEEE Trans. Antennas Propag.* **1999**, *47*, 1807–1813. [CrossRef]
9. Sarabandi, K.; Park, M. Extraction of Power Line Maps from Millimeter-Wave Polarimetric SAR Images. *IEEE Trans. Antennas Propag.* **2000**, *48*, 1802–1809. [CrossRef]
10. Xiong, W.; Luo, J.; Yu, C. Power Line Detection in Millimeter-Wave Radar Images Applying Convolutional Neural Networks. *IET Radar Sonar Navig.* **2021**, *15*, 1083–1095. [CrossRef]
11. Qirong, M.; Darren, S.G.; Yi-Chi, S.; Ming-Ting, S. An Algorithm for Power Line Detection and Warning Based on a Millimeter-Wave Radar Video. *IEEE Trans. Image Process.* **2011**, *20*, 3534–3543. [CrossRef] [PubMed]

12. Sarabandi, K.; Park, M. A Radar Cross-Section Model for Power Lines at Millimeter-Wave Frequencies. *IEEE Trans. Antennas Propag.* **2003**, *51*, 2353–2360. [CrossRef]
13. Gibson, W.C. *The Method of Moments in Electromagnetics*; Taylor & Francis: New York, NY, USA, 2021.
14. Chew, W.C.; Michielssen, E.; Song, J.M.; Jin, J.-M. *Fast and Efficient Algorithms in Computational Electromagnetics*; Artech House, Inc.: Norwood, MA, USA, 2001.
15. Kalfa, M.; Ergül, Ö.; Ertürk, V.B. Error Control of Multiple-Precision MLFMA. *IEEE Trans. Antennas Propag.* **2018**, *66*, 5651–5656. [CrossRef]
16. Sharma, S.; Triverio, P. AIMx: An Extended Adaptive Integral Method for the Fast Electromagnetic Modeling of Complex Structures. *IEEE Trans. Antennas Propag.* **2021**, *69*, 8603–8617. [CrossRef]
17. Seo, S.M. A Fast IE-FFT Algorithm to Analyze Electrically Large Planar Microstrip Antenna Arrays. *IEEE Antennas Wirel. Propag. Lett.* **2018**, *17*, 983–987. [CrossRef]
18. Zhao, K.; Vouvakis, M.N.; Lee, J.-F. The Adaptive Cross Approximation Algorithm for Accelerated Method of Moments Computations of EMC. *IEEE Trans. Electromagn. Compat.* **2005**, *47*, 763–773. [CrossRef]
19. Chen, C.; Yang, F.; Hu, C.; Zhou, J. An Improved RCS Calculation Method for Power Lines Combining Characteristic Mode with SMWA. *Electronics* **2022**, *11*, 2051. [CrossRef]
20. Peng, Z.; Lim, K.; Lee, J. A Discontinuous Galerkin Surface Integral Equation Method for Electromagnetic Wave Scattering From Nonpenetrable Targets. *IEEE Antennas Propag. Mag.* **2013**, *61*, 3617–3628. [CrossRef]
21. Zhang, L.; Sheng, X. A Discontinuous Galerkin Volume Integral Equation Method for Scattering from Inhomogeneous Objects. *IEEE Trans. Antennas Propag.* **2015**, *63*, 5661–5667. [CrossRef]
22. Rao, S.; Wilton, D.; Glisson, A. Electromagnetic Scattering by Surfaces of Arbitrary Shape. *IEEE Trans. Antennas Propag.* **1982**, *30*, 409–418. [CrossRef]
23. Angiulli, G.; Amendola, G.; Di Massa, G. Application of Characteristic Modes to the Analysis of Scattering from Microstrip Antennas. *J. Electromagn. Waves Appl.* **2000**, *14*, 1063–1081. [CrossRef]
24. Guan, L.; He, Z.; Ding, D.; Chen, R. Efficient Characteristic Mode Analysis for Radiation Problems of Antenna Arrays. *IEEE Trans. Antennas Propag.* **2019**, *67*, 199–206. [CrossRef]
25. Chen, X.; Gu, C.; Zhuo, L.; Niu, Z. Accelerated Direct Solution of Electromagnetic Scattering via Characteristic Basis Function Method With Sherman-Morrison-Woodbury Formula-Based Algorithm. *IEEE Trans. Antennas Propag.* **2016**, *64*, 4482–4486. [CrossRef]
26. Fang, X.; Cao, Q.; Zhou, Y.; Yi, W. Multiscale Compressed and Spliced Sherman–Morrison–Woodbury Algorithm With Characteristic Basis Function Method. *IEEE Trans. Electromagn. Compat.* **2017**, *60*, 716–724. [CrossRef]
27. Wang, K.; Li, M.; Ding, D.; Chen, R. A Parallelizable Direct Solution of Integral Equation Methods for Electromagnetic Analysis. *Eng. Anal. Bound. Elem.* **2017**, *85*, 158–164. [CrossRef]
28. Rong, Z.; Jiang, M.; Chen, Y.; Lei, L.; Li, X.; Nie, Z.; Hu, J. Fast Direct Solution of Integral Equations with Modified HODLR Structure for Analyzing Electromagnetic Scattering Problems. *IEEE Trans. Antennas Propag.* **2019**, *67*, 3288–3296. [CrossRef]
29. Ubeda, E.; Rius, J.M. Novel Monopolar MFIE MoM-Discretization for the Scattering Analysis of Small Objects. *IEEE Trans. Antennas Propag.* **2006**, *54*, 50–57. [CrossRef]
30. Ziegler, V.; Schubert, F.; Schulte, B.; Giere, A.; Koerber, R. Helicopter Near-Field Obstacle Warning System Based on Low-Cost Millimeter-Wave Radar Technology. *IEEE Trans. Microw. Theory Tech.* **2013**, *61*, 658–665. [CrossRef]
31. Kohmura, A.; Yonemoto, N.; Futatsumori, S.; Morioka, K. Evaluation of Polarisation Characteristics of Power-Line RCS at 76 GHz for Helicopter Obstacle Detection. *Electron. Lett.* **2015**, *51*, 1110–1111.